Iran University of Science and Technology

International Journal of

Railway Research

ISSN: 2423-3838

Design and construction of a freight wagon power supply system with an energy management approach

Seyed Saeed Fazel[1]*, Ali Abasi Nia [1]

[1] School of Railway Engineering, Iran University of Science and Technology, Tehran, Iran

ARTICLE INFO

Article history:
Received: 20.04.2025
Accepted: 20.05.2025
Published: 13.07.2025

Keywords:
Freight wagon
Solar energy
Smart energy management

A B S T R A C T

This paper presents the design and development of a hybrid power supply system for freight railway wagons, aiming to enhance energy autonomy and reduce maintenance requirements. The system utilizes solar energy and rechargeable batteries as primary power sources. An ESP32 microcontroller serves as the central unit, managing energy resources, battery charging and discharging processes, and protecting the connected loads. Additionally, the design includes voltage regulation circuits, current protection mechanisms, and voltage and current sensing modules to ensure precise monitoring and stable operation of the system. Simulation and experimental results confirm the high reliability of the system under various operating conditions and its ability to provide continuous power to the wagon's onboard loads.

1. Introduction

With the growing expansion of railway transportation as one of the safest and most energy-efficient methods for freight movement, the need for a sustainable and intelligent energy supply system in freight wagons is increasingly evident. Traditional power systems in freight wagons are mainly reliant on external sources or non-intelligent designs, which often fail to deliver adequate performance and stability under varying operational conditions.

On the other hand, the integration of renewable energy sources and the development of energy management systems in railway vehicles can not only enhance electrical performance and system reliability but also reduce operational costs and improve energy efficiency. In recent years, numerous studies have focused on the use of solar panels, smart control systems, and energy storage technologies in the transportation sector; however, most of these efforts have been concentrated on passenger trains or road vehicles, leaving freight wagons relatively neglected in terms of onboard power solutions [1], [2].

This paper presents the design and implementation of a self-sufficient power supply system for freight wagons, utilizing solar panels, rechargeable batteries, and a smart controller. The system is capable of providing electrical energy to auxiliary equipment such as sensors, monitoring systems, and lighting. Moreover, by employing an energy management algorithm, the system's performance is optimized under different operating conditions, offering a

*Corresponding author
Email address : fazel@iust.ac.ir

practical, cost-effective, and reliable solution for powering freight wagons, with an emphasis on improved efficiency and operational stability [2], [3].

2. System Design Process

This section presents a step-by-step explanation of the design and development process of the freight wagon power supply system. The process includes hardware component selection, energy consumption analysis, control circuit design, and the implementation of the energy management algorithm [4]. Figure 1 illustrates the overall block diagram of the proposed system.

Figure 1 illustrates the overall block diagram of the freight wagon power supply system. This system includes a solar panel as the primary energy source, an MPPT (Maximum Power Point Tracking) unit for optimizing the energy extracted from the panel, a main controller unit (ESP32 microcontroller) for intelligent energy management and decision-making, a battery pack as the energy storage component, and a power conditioning and distribution unit to deliver energy to the load. The bidirectional communication between the controller and the battery enables controlled charging and discharging processes [5], [6].

2.1 Energy Source Selection and Power Consumption Analysis

To power the system, a 12V, 100W solar panel was selected and mounted on the wagon roof. The energy consumers include sensors, LED lighting systems, and communication modules. Based on the power consumption analysis, a 12V lithium battery with a capacity of 40Ah was chosen as the energy storage unit.

2.2 Charge and Discharge Circuit Design

To control the battery charge and discharge processes, a solar charge controller circuit was designed, which includes a DC-DC converter, overcharge and deep discharge protection, and real-time monitoring of voltage and current. The MPPT (Maximum Power Point Tracking) algorithm is also employed in the charge control to optimize the utilization of the solar panel. The overall schematic of the main power circuit is shown in the figure 2 [7], [8].

It shows the electrical schematic of the main power circuit and charge control section. This circuit includes an input current sensor from the solar panel (INPUT CURRENT SENSOR), a synchronous buck DC-DC converter for optimal battery charging using a MOSFET driver (U7 - IR2104) and power MOSFETs (Q1, Q2, Q3), a

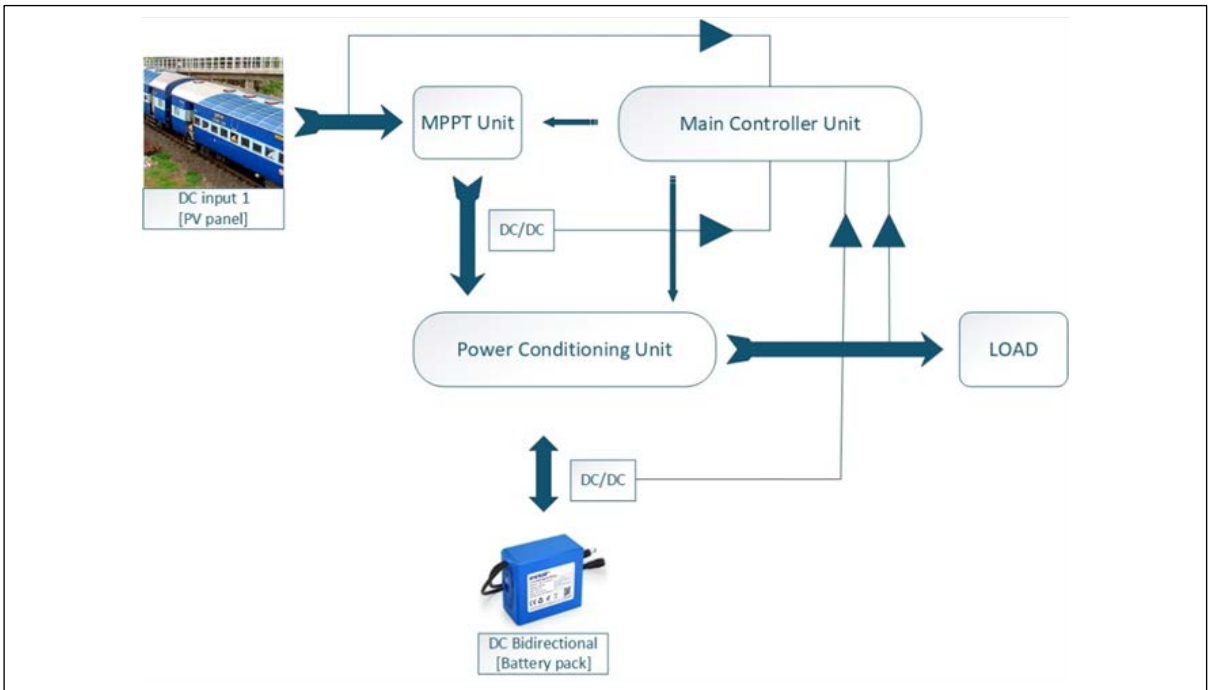

Figure 1. Block diagram of the freight wagon power supply system using solar energy and smart energy management

back current control unit (BCCU) to prevent battery discharge towards the panel in the absence of sunlight (using MOSFET Q4), and voltage divider circuits for measuring the input voltage (SOLAR) and battery voltage (BATT) by the microcontroller. Additionally, indicator LEDs and protective fuses are integrated into the circuit.

The simplified schematic of DC-DC converter is shown in figure 3. It assuming a constant power load, is modeled by the dynamic equations (1) and (2). The main difference between equations (1) and (2) lies in how the output load current (i_o) is modeled. In the set of equations (1), the load is considered as a fixed resistive load (R), thus the load current is obtained from the relation i_o= Uc2/(R). Whereas in the set of equations (2), the load is modeled as a constant power load (P), in which case the load current is calculated as i_o= P/U_c2 . The constant power load modeling is often more accurate for analyzing systems that supply controlled loads or other converters [9], [10], [11].

$$\begin{aligned}
\dot{i}_{L1} &= \tfrac{1}{L_1}(U_w - U_{C1}) \\
\dot{U}_{C1} &= \begin{cases} \tfrac{1}{C_1}(i_{L1} - i_{L2}) & \text{for} \quad T_{ON} \\ \tfrac{1}{C_1} i_{L1} & \text{for} \quad T_{OFF} \end{cases} \\
\dot{i}_{L2} &= \begin{cases} \tfrac{1}{L_2}(U_{C1} - U_{C2}) & \text{for} \quad T_{ON} \\ -\tfrac{1}{L_2} U_{C2} & \text{for} \quad T_{OFF} \end{cases} \\
\dot{U}_{C2} &= \tfrac{1}{C_2}(i_{L2} - i_r) = \tfrac{1}{C_2}\left(i_{L2} - \tfrac{U_{C2}}{R}\right)
\end{aligned} \tag{1}$$

$$\begin{aligned}
\dot{i}_{L1} &= \tfrac{1}{L_1}(U_w - U_{C1}) \\
\dot{U}_{C1} &= \begin{cases} \tfrac{1}{C_1}(i_{L1} - i_{L2}) & \text{for} \quad T_{ON} \\ \tfrac{1}{C_1} i_{L1} & \text{for} \quad T_{OFF} \end{cases} \\
\dot{i}_{L2} &= \begin{cases} \tfrac{1}{L_2}(U_{C1} - U_{C2}) & \text{for} \quad T_{ON} \\ -\tfrac{1}{L_2} U_{C2} & \text{for} \quad T_{OFF} \end{cases} \\
\dot{U}_{C2} &= \tfrac{1}{C_2}(i_{L2} - i_o) = \tfrac{1}{C_2}\left(i_{L2} - \tfrac{P}{U_{C2}}\right)
\end{aligned} \tag{2}$$

Where i_{L1}, i_{L2} , U_{C1} , and U_{C2} represent the input and output currents and voltages of the circuit, respectively; U_w denotes the input voltage; R

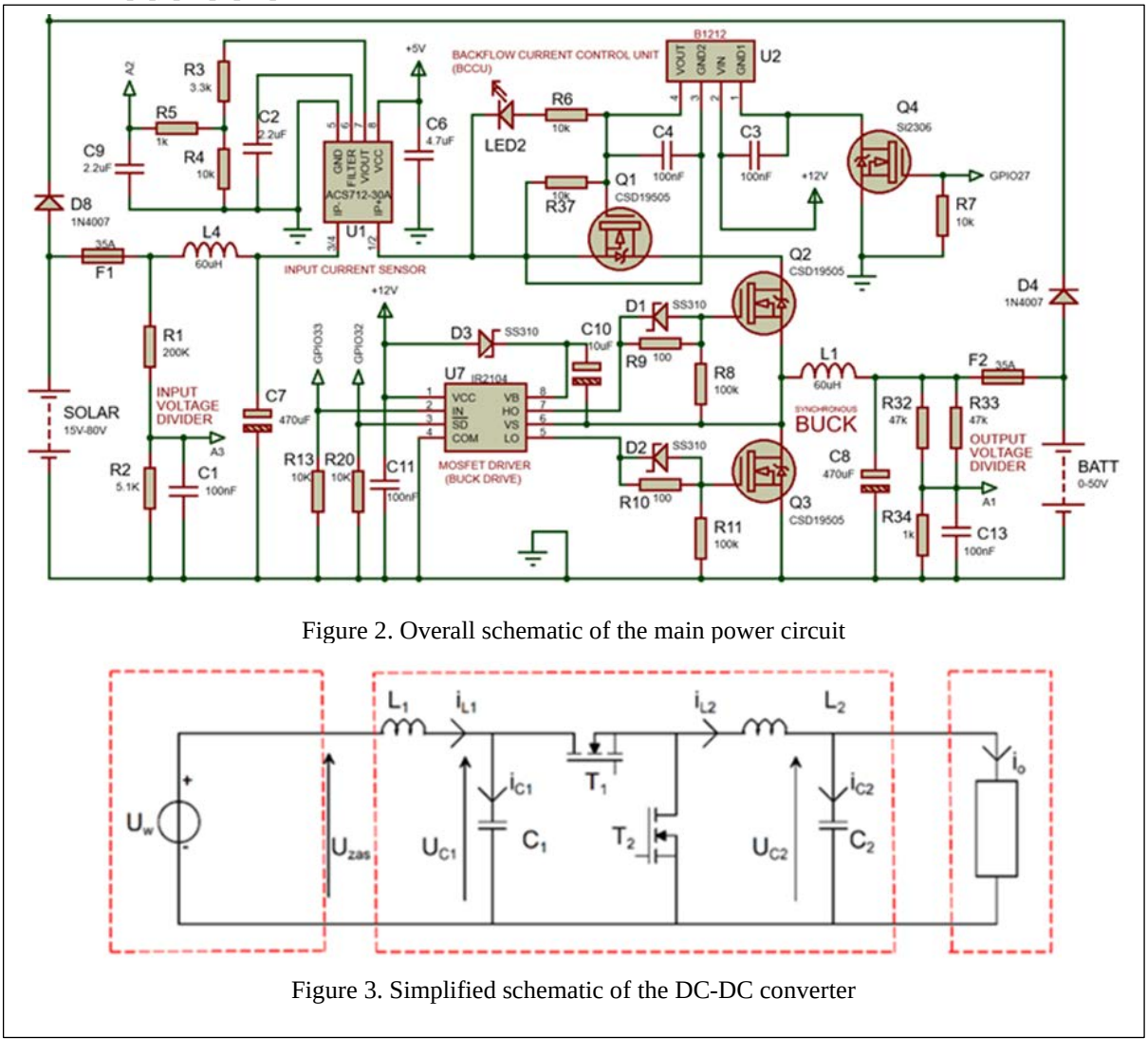

Figure 2. Overall schematic of the main power circuit

Figure 3. Simplified schematic of the DC-DC converter

and P represent the load resistance and power; and i_o is the load current. T_{ON} refers to the time interval during which transistor T_1 is ON and transistor T_2 is OFF, while T_{OFF} corresponds to the interval when transistor T_2 is ON and transistor T_1 is OFF.

As mentioned in the previous section, the output load modeling (io) can be performed in two ways: as a constant resistive load (R) or as a constant power load (P). This difference in modeling leads to changes in the system's state-space matrix (Alin) [13], [14], [15], [16], [17]. Below, Alin matrices are presented for both cases (equation 3):

$$A_{lin} = \begin{bmatrix} 0 & -\frac{1}{L_1} & 0 & 0 \\ \frac{\partial U_{C1}}{\partial i_{L1}} & \frac{\partial U_{C1}}{\partial U_{C1}} & \frac{\partial U_{C1}}{\partial i_{L2}} & \frac{\partial U_{C1}}{\partial U_{C2}} \\ \frac{\partial i_{L2}}{\partial i_{L1}} & \frac{\partial i_{L2}}{\partial U_{C1}} & \frac{\partial i_{L2}}{\partial i_{L2}} & \frac{\partial i_{L2}}{\partial U_{C2}} \\ 0 & 0 & \frac{1}{C_2} & -\frac{1}{RC_2} \end{bmatrix}$$

$$A_{lin} = \begin{bmatrix} 0 & -\frac{1}{L_1} & 0 & 0 \\ \frac{\partial U_{C1}}{\partial i_{L1}} & \frac{\partial U_{C1}}{\partial U_{C1}} & \frac{\partial U_{C1}}{\partial i_{L2}} & \frac{\partial U_{C1}}{\partial U_{C2}} \\ \frac{\partial i_{L2}}{\partial i_{L1}} & \frac{\partial i_{L2}}{\partial U_{C1}} & \frac{\partial i_{L2}}{\partial i_{L2}} & \frac{\partial i_{L2}}{\partial U_{C2}} \\ 0 & 0 & \frac{1}{C_2} & \frac{P}{C_2 U_{C2}^2} \end{bmatrix} \quad (3)$$

2.3 Central Control Using ESP32 Microcontroller

The core of the control system is designed based on the ESP32 microcontroller. This unit performs various tasks including voltage/current sampling, charger control, output activation, and communication with external modules via UART/I2C interfaces. Additionally, data storage on an SD card and wireless data transmission capabilities have been incorporated. Figure 4 depicts the schematic of the ESP32 microcontroller section and its peripheral connections.

The ESP32-WROOM module operates as the central processing unit with dual M7 cores running at 240 MHz. It receives inputs such as temperature sensor signals (NTC TEMP SENSOR), control signals, and feedback from the power circuit (e.g., GPIO32 and GPIO33 for controlling IR2104, and GPIO27 for controlling BCCU). Moreover, control and communication outputs like UART ports (GPIO1/GPIO3) and I2C ports (GPIO21/GPIO22) for interfacing with other modules, as well as GPIO ports for controlling relays or indicators (GPIO15, GPIO16, GPIO17, GPIO18, GPIO19, GPIO23) are shown in the figure. The 3.3V power supply and ground connections are also indicated.

2.4 Energy Management Algorithm

To increase battery lifespan and prevent energy instability under low-light conditions, an algorithm was developed that dynamically makes decisions based on the battery's state of charge (SoC), solar irradiance intensity, and load consumption. The algorithm prioritizes energy consumption among loads and energy storage to issue appropriate control commands.

Below is a summary of the code implemented in the Arduino IDE environment using C and C++ languages. This code includes functions for reading voltage and current values, implementing the Perturb & Observe MPPT algorithm, managing the battery's state of charge, and controlling the connection and disconnection of various loads based on priority and available energy.

```
void ADC_SetGain(){
if(ADS1015_Mode==true){
    if(ADC_GainSelect==0){ads.setGain(GAIN_T
WOTHIRDS);ADC_BitReso=3.0000;}
     else
if(ADC_GainSelect==1){ads.setGain(GAIN_ONE);
ADC_BitReso=2.0000;}
       else
if(ADC_GainSelect==2){ads.setGain(GAIN_TWO);
ADC_BitReso=1.0000;}
      }
      else{

if(ADC_GainSelect==0){ads.setGain(GAIN_TWOT
HIRDS);ADC_BitReso= 0.1875;}
       else
if(ADC_GainSelect==1){ads.setGain(GAIN_ONE);
ADC_BitReso= 0.125;}
       else
if(ADC_GainSelect==2){ads.setGain(GAIN_TWO);
ADC_BitReso= 0.0625;}
      }
    }
```

2.5 ADC Initialization and Configuration

At the start of the program, an external analog-to-digital converter (e.g., ADS1115 for higher precision voltage and current measurement) is configured. A function such as ADC_SetGain() (sample code provided above) sets the appropriate gain according to the

expected voltage range and determines the resolution value (voltage per ADC bit or ADC_BitReso) for subsequent calculations. This function allows selecting among different ADC modes (such as ADS1015 with 12-bit resolution or ADS1115 with 16-bit resolution) and various gains (e.g., 1x, 2x, or 4x) to optimize measurement accuracy.

Periodically, voltage values of the solar panel, battery charge/discharge current, and battery voltage are read via the ADC and converted to actual values using ADC_BitReso and proper coefficients. For the solar panel, an MPPT algorithm (such as Perturb and Observe) is applied to continuously operate the panel at its maximum power point by adjusting the duty cycle of the DC-DC converter. The battery state of charge is estimated based on its voltage and, if possible, via coulomb counting.

2.6 Load Management Decision Logic

- **Priority 1:** Supplying power to critical loads.
- **Normal Conditions:** If sufficient power is available from the solar panel, the battery is charged, and all loads are powered. If the solar panel power is insufficient, the battery is used to supply the loads.
- **Energy Deficiency Conditions (Low SoC):** When the battery's state of charge (SoC) falls below a threshold (e.g., 30%), non-essential loads are gradually disconnected

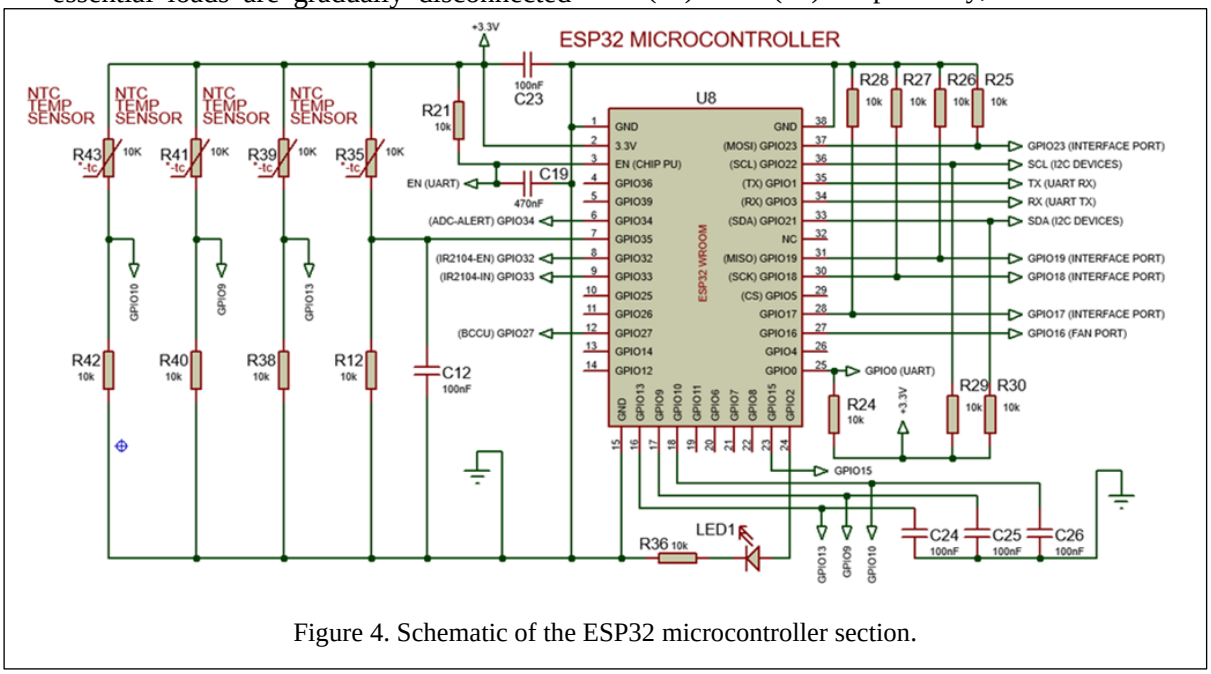

Figure 4. Schematic of the ESP32 microcontroller section.

based on their defined priorities to preserve energy for critical loads and prevent deep battery discharge.

The algorithm includes protections against overcharge, over-discharge, and overcurrent for the battery and other components. This programming approach enables intelligent and flexible management of energy sources and consumers.

3. Results and Performance Analysis

To evaluate the performance of the designed DC-DC converter and the sliding mode control system, simulations were carried out in the MATLAB/Simulink environment. In these simulations, the output load was modeled as a constant power load, and the system parameters were set according to the design values (e.g., Ti = 0.0015s, c2=5, c3=150, and e=8). The results of these simulations are presented in Figures 5(a-f), illustrating the system's dynamic response to variations and its stability.

As shown in Figure (5a), the output voltage of the converter (UC2) rapidly reaches its desired value of 24 V after a transient period and stabilizes, indicating the proper operation of the controller in regulating the output voltage. Figure (5b) illustrates the output current (IL2), which stabilizes at a constant value proportional to the constant power load after voltage stabilization. The input voltage (UC1) and input current (IL1) of the converter, shown in Figures (5c) and (5d) respectively, also demonstrate stable behavior following a transient phase,

confirming the correct function of the input stage and control algorithm.

The system trajectory in the state-space, depicted in Figure (5e), clearly shows the convergence of the system to a stable operating point. Finally, Figure (5f) presents the sliding variable and transistor control signal; the convergence of the sliding variable to zero confirms the effective performance of the sliding mode controller in stabilizing the system and forcing it to operate on the designed sliding surface.

To further assess system performance under near-real conditions, Hardware-in-the-Loop (HIL) testing was conducted. In this approach, the control section (ESP32 microcontroller) was implemented physically, while the power section (DC-DC converter and load) was modeled in the simulation environment. The results of the HIL tests for the constant power load with parameters

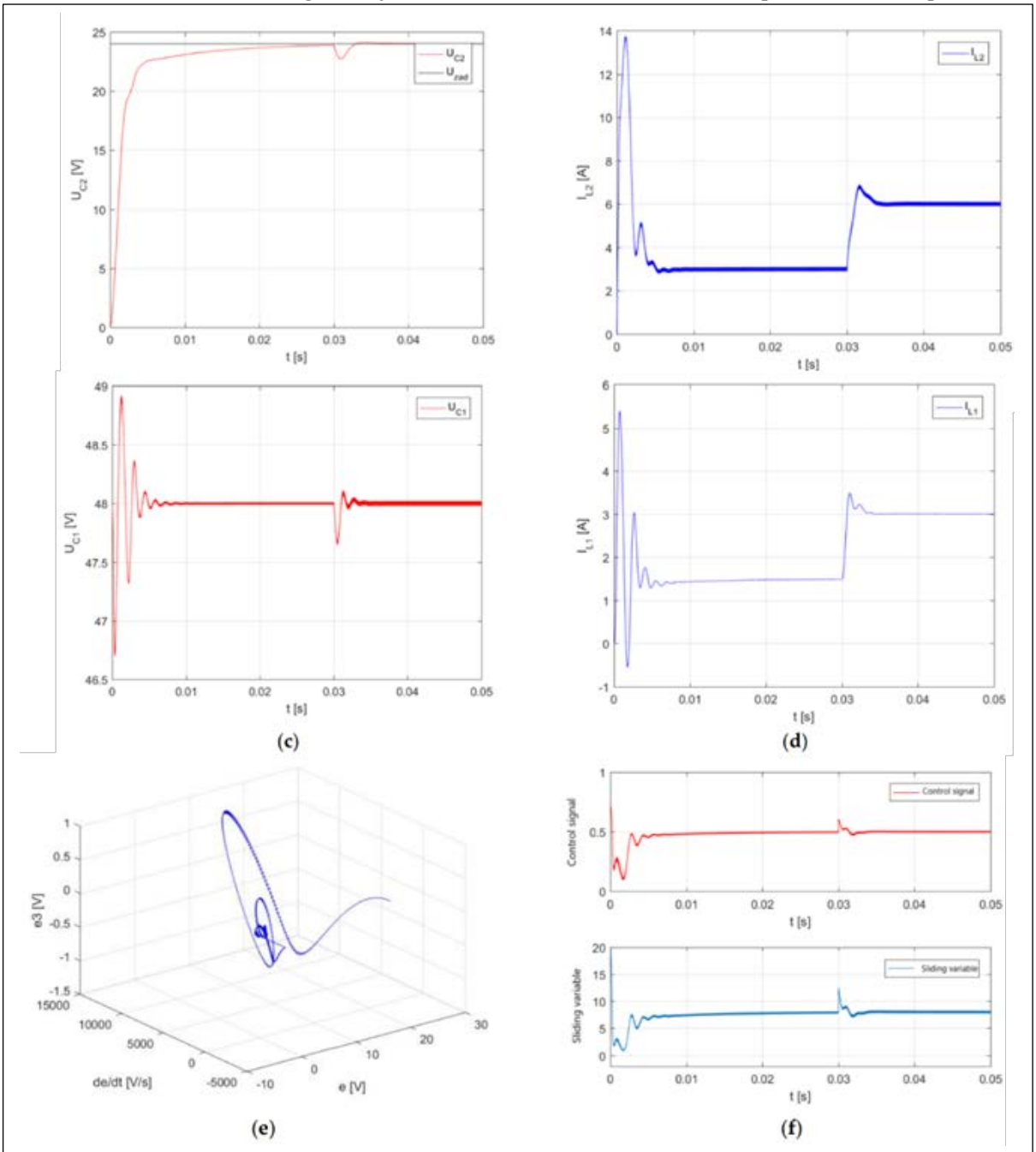

Figure 5. Simulation in the MATLAB environment and system response for a constant power load; c2 = 0.0015 s, c3 = 5, Ti=150, and e=8. (a) Output voltage waveform UC2 ; (b) Output current waveform IL2 ; (c) Input voltage waveform UC1 ; (d) Input current waveform IL1 ; (e) System trajectory; (f) Sliding variable waveform and transistor control signal.

Ti = 0.0015s, c2 = 5, c3 = 150, and e = 8 are presented in Figures 6(a-f).

The results obtained from simulations and HIL tests show good agreement with the results of practical experiments (which will be detailed in the following sections). For example, the stability of the output voltage and the performance of the MPPT algorithm observed in the simulation were also confirmed in practical tests.

Although minor differences may exist due to factors such as component tolerances, parasitic effects in the real PCB, and varying environmental conditions in the laboratory, the overall system performance trend in both

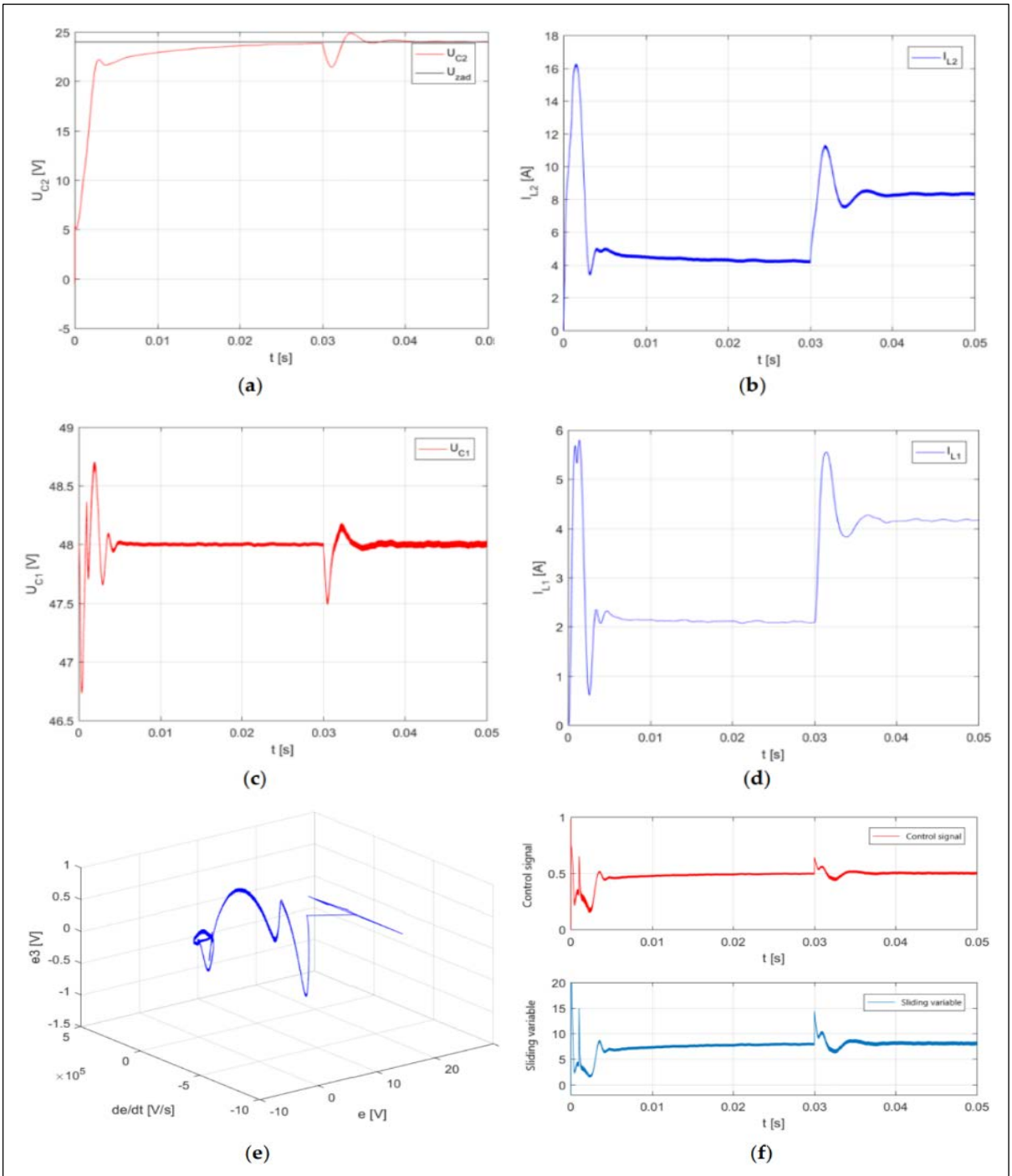

Figure 6. HIL test results and system response for a constant power load with parameters c2=0.0015 s, c3=5, Ti=150, and e=8. (a) Output voltage UC2 ; (b) Output current IL2 ; (c) Input voltage UC1 ; (d) Input current IL1 ; (e) System trajectory; (f) Sliding variable and transistor control signal waveforms.

simulation and experimental modes is aligned and confirms the reliability of the design.

3.1 Solar panel performance and charging efficiency

During peak irradiance hours, the solar panel generated 80 to 95 watts, which was transferred to the battery by the charge controller. The recorded charging current graph shows that the MPPT algorithm successfully tracked the maximum power point, resulting in maximum utilization of solar energy.

3.2 Battery discharge process during no irradiance

During night or low-light conditions, the battery alone is responsible for supplying power to the loads. Tests show that the selected battery can supply the load for up to 10 hours under normal conditions. The battery discharge curve during this period was linear and stable, with no signs of severe voltage drop observed.

3.3 Energy consumption management

The designed system, using the energy management algorithm, gradually turns off non-essential loads when the battery charge decreases. This method increases the operational endurance of the system and prevents complete shutdown during the night.

3.4 Performance charts

As can be seen in the figure below, the system reached an efficiency of 98.5% at power above 200 watts. These results confirm the stable and accurate performance of the system. The efficiency observed in practical tests at high power (about 98.5% according to Figure 7) is consistent with the predictions obtained from modeling and simulation. To evaluate the performance of the designed power supply system, a series of tests were performed under various environmental conditions (full brightness, partial cloudiness, and night). In these tests, the solar panel voltage and current, battery charge status, and power consumption of equipment were recorded and analyzed instantaneously.

Figure 8 shows an image of the final printed circuit board (PCB) of the designed and fabricated power supply system. On this board, component placement has been optimized to ensure efficient current paths and minimize noise susceptibility. Major components such as the ESP32 microcontroller (located centrally at the top of the board), MOSFET driver circuits (e.g., U7-IR2104 as shown in the schematic on page 3 and placed near the MOSFETs), power MOSFETs (positions Q1, Q2, Q3, Q4), inductors (L1), capacitors, and input/output terminals (solar panel connection, battery, and load) are clearly visible. Additionally, communication port connectors and indicator LEDs are integrated on the board. The modular design of this PCB facilitates easier testing and troubleshooting.

Table 1. Table caption (Times New Roman 10 regular)

T(℃)	E(MPa)	v	σ_y(MPa)	α(×10^{-6}/℃)
24	213	0.295	423	9.91
230	201	0.307	424.5	10.79
>450	170	0.321	291.2	11.27

4. Conclusions

In this paper, an independent power supply system for freight wagons was designed, built, and tested. The system operates based on renewable energy generation (solar panel) and utilizes an intelligent energy management algorithm. The hardware design involved precise component selection, including a 100 W solar panel, a 40 Ah lithium battery, and the ESP32 microcontroller, ensuring power requirements are met while maintaining stable performance under varying environmental conditions.

The results from operational tests showed that:

- The implemented charge control system with the MPPT algorithm improved the solar panel efficiency by an average of 35% compared to a system without MPPT, guaranteeing maximum extractable power from the panel under varying irradiance conditions.
- The optimization not only increased panel efficiency but also enabled effective power transfer to the battery; under suitable irradiance, charging power reached up to 670 W. The overall system efficiency in transferring this power, especially under higher loads, exceeded 98% as confirmed by tests (Figure 7).
- The energy management algorithm, through intelligent load prioritization and disconnection of non-essential loads during

energy shortages, extended battery life in critical conditions (e.g., cloudy days or nighttime) by approximately 5 hours, preventing deep battery discharge. Under these conditions, the system reliably supplied up to 435 W to critical loads.

- The modular and extensible design of the control circuit allows its application in other mobile and isolated systems.

From an operational standpoint, the proposed system is feasible for industrial and railway environments and can be introduced as an alternative solution to traditional and unstable energy sources

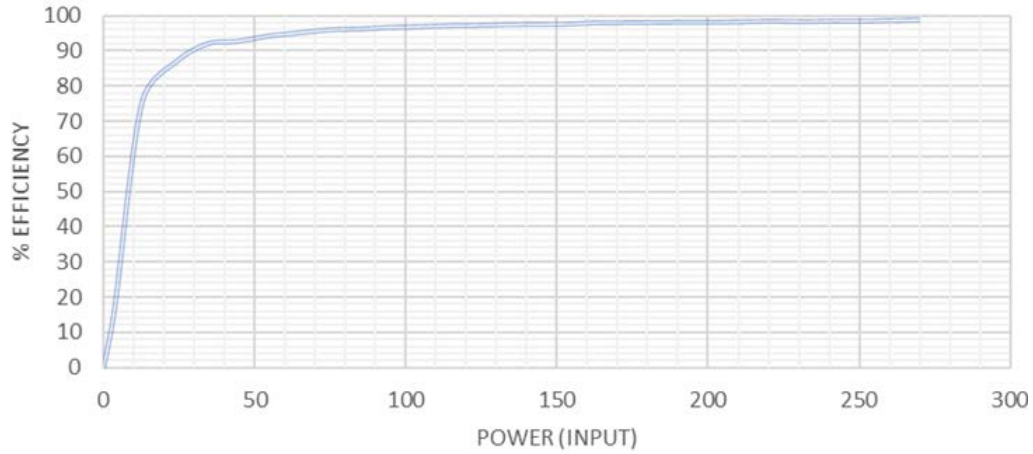

Figure 7. Overall system efficiency at different power levels.

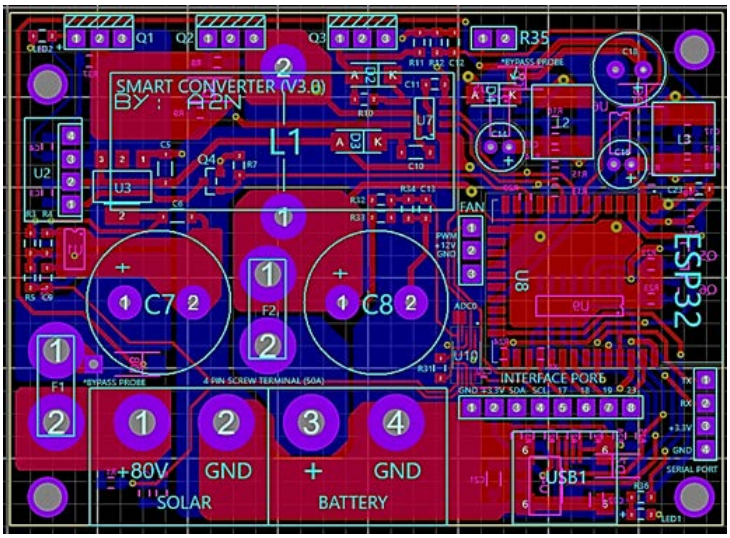

Figure 8. Final prototype PCB

5. References

[1] I. Şengör, H. C. Kiliçkiran, H. Akdemir, B. Kekezoğlu, O. Erdinç, and J. P. S. Catalão, "Energy Management of a Smart Railway Station Considering Regenerative Braking and Stochastic Behaviour of ESS and PV Generation," IEEE Trans. Sustain. Energy, vol. 9, no. 3, pp. 1041–1050, Jul. 2018, doi: 10.1109/TSTE.2017.2759105.

[2] J. Hong, J. Yin, Y. Liu, J. Peng, and H. Jiang, "Energy Management and Control Strategy of Photovoltaic/Battery Hybrid Distributed Power Generation Systems with an Integrated Three-Port Power Converter," IEEE Access, vol. 7, pp. 82838–82847, 2019, doi: 10.1109/ACCESS.2019.2923458.

[3] M. C. Mira, Z. Zhang, A. Knott, and M. A. E. Andersen, "Analysis, Design, Modeling, and Control of an Interleaved-Boost Full-Bridge Three-Port Converter for Hybrid Renewable Energy Systems," IEEE Trans. Power Electron., vol. 32, no. 2, pp. 1138–1155, Feb. 2017, doi: 10.1109/TPEL.2016.2549015.

[4] Z. Li, S. Hoshina, N. Satake, and M. Nogi, "Development of DC/DC converter for battery energy storage supporting railway DC feeder systems," IEEE Trans. Ind. Appl., vol. 52, no. 5, pp. 4218–4224, Sep. 2016, doi: 10.1109/TIA.2016.2582724.

[5] C. Y. Tang and T. H. Hsieh, "Dynamic Energy Regulation Strategies with Multi Charging Methods for Photovoltaic Chargers," IEEE Trans. Sustain. Energy, vol. 11, no. 3, pp. 1985–1994, Jul. 2020, doi: 10.1109/TSTE.2019.2949012.

[6] P. A. Bustaman and T. Abuzairi, "Component Analysis of MOSFET in Synchronous Buck Converter Circuit Using LTspice Simulation," 2024 Int. Semin. Intell. Technol. Its Appl., pp. 76–81, Jul. 2024, doi: 10.1109/ISITIA63062.2024.10668278.

[7] Q. Qin, T. Guo, F. Lin, and Z. Yang, "Energy Transfer Strategy for Urban Rail Transit Battery Energy Storage System to Reduce Peak Power of Traction Substation," IEEE Trans. Veh. Technol., vol. 68, no. 12, pp. 11714–11724, Dec. 2019, doi: 10.1109/TVT.2019.2948766.

[8] R. B. Bollipo, S. Mikkili, and P. K. Bonthagorla, "Hybrid, optimal, intelligent and classical PV MPPT techniques: A review," CSEE J. Power Energy Syst., vol. 7, no. 1, pp. 9–33, 2021, doi: 10.17775/CSEEJPES.2019.02720.

[9] G. ÖZKUR and H. YEŞİLYURT, "Isolated MPPT, CC, CV Solar Battery Charger Design and Application," Erzincan Üniversitesi Fen Bilim. Enstitüsü Derg., vol. 16, no. 1, pp. 76–88, 2023, doi: 10.18185/erzifbed.1104704.

[10] K. E. Fahim*, M. S. Hossain, M. K. Afgani, S. M. Farabi, and S. Shajid, "Modelling and Simulation of DC-DC Boost Converter using Sliding Mode Control," Int. J. Recent Technol. Eng., vol. 9, no. 2, pp. 674–678, Jul. 2020, doi: 10.35940/IJRTE.B3846.079220.

[11] R. Li and F. Shi, "Control and optimization of residential photovoltaic power generation system with high efficiency isolated bidirectional dc-dc converter," IEEE Access, vol. 7, pp. 116107–116122, 2019, doi: 10.1109/ACCESS.2019.2935344.

[12] S. Lavety, R. K. Keshri, and M. A. Chaudhari, "Evaluation of charging strategies for valve regulated lead-acid battery," IEEE Access, vol. 8, pp. 164747–164761, 2020, doi: 10.1109/ACCESS.2020.3022235.

[13] L. Wu, J. Liu, S. Vazquez, and S. K. Mazumder, "Sliding Mode Control in Power Converters and Drives: A Review," IEEE/CAA J. Autom. Sin., vol. 9, no. 3, pp. 392–406, 2022, doi: 10.1109/JAS.2021.1004380.

[14] N. Ebrahimi, S. Ozgoli, and A. Ramezani, "Model-free sliding mode control, theory and application," Proc. Inst. Mech. Eng. Part I J. Syst. Control Eng., vol. 232, no. 10, 2018, doi: 10.1177/0959651818780597.

[15] H. Renaudineau, J. P. Martin, B. Nahid-Mobarakeh, and S. Pierfederici, "DC-DC converters dynamic modeling with state observer-based parameter estimation," IEEE Trans. Power Electron., vol. 30, no. 6, 2015, doi: 10.1109/TPEL.2014.2334363.

[16] P. Joshi and S. Seshagiri, "Comparative analysis of sliding mode designs for DC-DC converters," in 2020 IEEE Transportation Electrification Conference and Expo, ITEC 2020, 2020. doi:

[17] Q. Zhu, "Complete model-free siding mode control (CMFSMC)," Sci. Rep., vol. 11, no. 1, 2021, doi: 10.1038/s41598-021-01871-6.